

NMR Mapping of the IFNAR1-EC Binding Site on IFN α 2 Reveals Allosteric Changes in the IFNAR2-EC Binding Site[†]

Sabine Ruth Akabayov,^{‡,||} Zohar Biron,[‡] Peter Lamken,[§] Jacob Piehler,^{§,⊥} and Jacob Anglister^{*‡}

[‡]Department of Structural Biology, Weizmann Institute of Science, Rehovot 76100, Israel and [§]Institute of Biochemistry, Johann Wolfgang Goethe University, Frankfurt am Main, Germany ^{||}Present address: Department of Biological Chemistry and Molecular Pharmacology, Harvard Medical School, 240 Longwood Ave., Boston, MA 02115. [⊥]Present address: Department of Biophysics, University of Osnabrück, Barbarastr. 11, 49076 Osnabrück, Germany.

Received July 29, 2009; Revised Manuscript Received December 4, 2009

ABSTRACT: All type I interferons (IFNs) bind to a common cell-surface receptor consisting of two subunits. IFNs initiate intracellular signal transduction cascades by simultaneous interaction with the extracellular domains of its receptor subunits, IFNAR1 and IFNAR2. In this study, we mapped the surface of IFN α 2 interacting with the extracellular domain of IFNAR1 (IFNAR1-EC) by following changes in or the disappearance of the ¹H–¹⁵N TROSY-HSQC cross peaks of IFN α 2 caused by the binding of the extracellular domain of IFNAR1 (IFNAR1-EC) to the binary complex of IFN α 2 with IFNAR2-EC. The NMR study of the 89 kDa complex was conducted at pH 8 and 308 K using an 800 MHz spectrometer. IFNAR1 binding affected a total of 47 of 165 IFN α 2 residues contained in two large patches on the face of the protein opposing the binding site for IFNAR2 and in a third patch located on the face containing the IFNAR2 binding site. The first two patches form the IFNAR1 binding site, and one of these matches the IFNAR1 binding site previously identified by site-directed mutagenesis. The third patch partially matches the IFN α 2 binding site for IFNAR2-EC, indicating allosteric communication between the binding sites for the two receptor subunits.

Type I interferons (IFNs)¹ make up a family of homologous helical cytokines that constitute a major component of the innate immune response (1). This family consists of 13 IFN α isotypes as well as single forms of IFN β , IFN ϵ , IFN κ , and IFN ω (1). IFNs initiate a strong antiviral and antiproliferative activity and provide the first line of defense against viral infection. All human type I IFNs share a common cell-surface receptor consisting of two subunits, IFNAR1 and IFNAR2 (2, 3). The extracellular domain of the IFNAR2 subunit (IFNAR2-EC) binds IFNs with high affinity [K_D = 10 nM for IFN α 2 (4)] in the absence of the extracellular domain of IFNAR1 (IFNAR1-EC). The affinity of the human IFNAR1-EC subunit for IFNs is much lower with a K_D for IFN α 2 of 5 μ M (5). IFN-induced association of the receptor subunits results in reciprocal transphosphorylation of the IFNAR1-associated Tyk2 protein and the IFNAR2-associated Jak1 protein. These processes initiate an intracellular signal transduction cascade leading to strong antiviral and antiproliferative responses (6–11).

Several mechanisms, involving preassociation of the receptor chains and ligand-induced changes, were postulated on the basis of other cytokine receptor systems (6–11). Studies of the receptor subunits tethered to solid-supported lipid bilayers confirmed a two-step binding mechanism in which IFN binds first to IFNAR2-EC and then recruits IFNAR1-EC to form the ternary complex (12, 13). High-resolution three-dimensional structures of the ternary complex formed by IFNAR1-EC, IFNAR2-EC, and any one of the type I IFNs as well as of the structure of the individual proteins and that of a IFNAR2-EC/IFN heterodimer should enhance our understanding of how the various IFNs differ in their mode of binding to IFNAR1-EC and IFNAR2-EC and help us to understand the initial steps in interferon signaling. At present, atomic-resolution structures of the ternary complex and IFNAR1-EC–IFN and IFNAR2-EC–IFN heterodimers are not known. However, the structures of three IFN molecules, IFN α 2, IFN β , and IFN τ , were determined by X-ray crystallography and NMR (14–18), revealing a bundle of five anti-parallel helices. The structure of IFNAR2-EC was determined using multidimensional NMR techniques. This structure consists of two perpendicular fibronectin domains connected by a rigid hinge region (19, 20).

In the absence of high-resolution three-dimensional structures of the binary and ternary complexes formed by IFNs and the receptor subunits, several laboratories have attempted to map the binding interfaces on IFNAR2-EC, IFN α / β , and IFNAR1-EC. Mutational analysis of IFNAR2-EC identified four receptor residues in the β 3– β 4 loop as “hot spots” for IFN α 2 binding, with some contributions from residues in the β 5– β 6 loop and the hinge region (4). In a parallel study, mutations of IFNAR2-EC residue E77 in the β 5– β 6 loop and of three residues in the hinge region were found to abolish the response to IFN α 2 with no

[†]This study was supported by the Israel Science Foundation, National Institutes of Health Grant GM53329, and the Kimmelman Center. J.A. is the Dr. Joseph and Ruth Owades Professor of Chemistry.

*To whom correspondence should be addressed. E-mail: Jacob.anglister@weizmann.ac.il. Phone: 972-8-9343394. Fax: 972-8-9344136.

^{||}Abbreviations: D1–D4, first through fourth fibronectin subdomains in the extracellular region of IFNAR1, respectively; $\Delta\delta$, chemical shift difference; EM, electron microscopy; EPO, erythropoietin; hGH, human growth hormone; HSQC, heteronuclear single-quantum coherence; IFN, interferon; IFNAR1-EC, extracellular domain of subunit 1 of the receptor for α - and β -interferons; IFNAR2-EC, extracellular domain of subunit 2 of the receptor for α - and β -interferons; IL-4, interleukin-4; Jak1, Janus kinase 1; K_D , equilibrium dissociation constant; NOE, nuclear Overhauser enhancement; TROSY, transverse relaxation-optimized spectroscopy; Tyk2, tyrosine kinase 2. A U preceding a molecule's name indicates an unlabeled molecule.

effect on the response to IFN β (21). Double-mutant cycle experiments revealed interactions between five IFNAR2-EC residues and corresponding IFN α 2 residues (22).

Changes in IFNAR2-EC ^1H and ^{15}N amide chemical shifts upon IFN α 2 binding were also used to map the IFN α 2 binding site on IFNAR2-EC (34). This binding site was found to be formed by a strip of hydrophobic residues flanked by two strips of polar residues. Overall, the binding site for IFN α 2 consists of the β 3– β 4 loop, the beginning of the β 5– β 6 loop, the end of the β 6 strand, and the hinge region of IFNAR2-EC. NMR mapped the binding site for IFN α 2 on IFNAR2-EC to an area larger than that identified previously by mutational studies and included most residues previously implicated in IFN α 2 binding.

Even before the three-dimensional structure of IFN α 2 was available, the AB loop and the D helix of the cytokine were identified as being important for IFN activity and for its interactions with IFNAR2-EC. Knowledge of the structure of IFN α 2 (16, 17) provided the basis for additional mutational studies of the binding site for IFNAR2-EC on IFN α 2. Several IFN α 2 residues were identified as the hot spot residues for the cytokine binding site of IFNAR2-EC (4). Residues in the AB loop, the D helix, the DE loop, and the E helix were also found to be involved in IFNAR2-EC binding (4, 22, 23). NMR studies revealed the entire continuous surface of IFN α 2 involved in IFNAR2-EC binding (24). Overall, the NMR analysis mapped the IFN α 2 binding site for IFNAR2-EC to the AB loop, and the E helix of the cytokine. The NMR mapping is in a good agreement with the earlier mutational results (22, 23) and highlights additional residues as being part of the IFN α 2 binding site for IFNAR2-EC.

The binding site for IFNAR1-EC on IFN α 2 has been investigated by site-directed mutagenesis. This site was mapped to the B and C helices on IFN α 2 opposite to the IFN α 2 binding site for IFNAR2-EC (25). This is similar to what has been shown for hGH, EPO, and IL4 where the cytokine binds to two receptor subunits through two distinct binding surfaces on opposing faces of the cytokines (26). Mutations of residues F64, N65, and T69 in the B helix and L80, Y85, and Y89 in the C helix were found to reduce the level of binding to IFNAR1-EC or reduce the biological activity of IFN α 2 by more than 2-fold (25, 27, 28). R120 was previously identified to be involved in IFNAR1 binding. Mutation of R120 to alanine decreased antiviral activity to 1–3% and antiproliferative activity to ~0.05%, and the R120E charge-reversal mutation led to a total loss of activity (29). In contrast, mutations of H57, E58, and Q61 on the B helix to alanine were found to increase the level of binding to IFNAR1-EC (25) and specifically enhanced its antitumor activity (30, 31). IFN α 2 mutants H57Y, E58N, and Q61S were found to be optimal for IFNAR1-EC binding and were similar in their activity and binding properties to IFN β (31).

IFNAR1-EC consists of four fibronectin domains (D1–D4), and the three N-terminal domains were implicated in IFN binding (5). Site-directed mutagenesis studies have shown that residues in D2 and D3 participate in the formation of the binding site for IFN α 2 (32). The $^{62}\text{FSSSLKLN}^{70}$ segment in D1 was identified as being involved in IFN binding and in the induction of biological activity (33).

Different models for the IFN α 2 complex with IFNAR2-EC have been calculated (22, 24). The model incorporating the most recent experimental data used the NMR mapping of the binding sites of IFNAR2-EC and IFN α 2, NOEs between D35 of IFN α 2 and K48 of IFNAR2-EC, and previously published

double-mutant cycle constraints (22) to dock IFN α 2 into the IFNAR2-EC binding site using the three-dimensional NMR structures of the two molecules (24). In all these models, the N-terminal domain and the hinge region of IFNAR2-EC interact with a complementary surface on IFN α 2.

A low-resolution structure of the IFNAR2-EC–IFN α 2–IFNAR1-EC ternary complex was obtained recently using electron microscopy (34). The NMR-based model of the IFNAR2-EC–IFN α 2 complex (24) was compatible with this EM structure without any modifications. Homology modeling was used to calculate a model for IFNAR1-EC that was fitted into the EM structure as well (34). The EM-based model for the ternary complex suggested that the three N-terminal fibronectin domains of IFNAR1-EC (D1, D2, and D3) interact with IFN while the fourth extracellular domain of IFNAR1-EC (C-terminal) interacts with the second (C-terminal) domain of IFNAR2-EC.

In this study, we use NMR spectroscopy to determine the entire binding site for IFNAR1-EC on IFN α 2 and probe changes in IFN α 2 upon binding of IFNAR1-EC to the binary complex between IFN α 2 and IFNAR2-EC. The mapping of the binding site for IFNAR1-EC on IFN α 2 reveals two adjacent binding surfaces for IFNAR1-EC, one of which is in excellent agreement with mutational data and the other of which is a new region that was not previously revealed in mutational analyses. In addition to changes in chemical shift that are associated with the IFN α 2 binding surface for IFNAR1-EC, significant changes were observed also in the IFN α 2 face containing the binding site for IFNAR2-EC. These changes indicate that IFNAR1-EC binding causes allosteric changes in the binding site for IFNAR2-EC. This communication between the two binding sites found on opposing surfaces of IFN α 2 could be important for the mutual orientation of the two receptor subunits for the initiation of the intracellular signal transduction cascade.

EXPERIMENTAL PROCEDURES

Uniformly ^{15}N - and ^2H -labeled IFN α 2, unlabeled IFNAR2-EC (U-IFNAR2-EC), and unlabeled IFNAR1-EC (U-IFNAR1-EC) were expressed and purified as described previously (24, 35). IFNAR1-EC in its truncated form that contains D1, D2, and D3 was prepared as previously described (5).

IFNAR2-EC and IFN α 2 at a 1:1:1 molar ratio and at a concentration of approximately 0.5 μM were incubated for 1–2 h in a 25 mM deuterated Tris solution (pH 8) containing 0.02% NaN_3 . For the formation of the ternary complex, IFNAR1-EC was added to the 0.5 μM solution of the IFNAR2-EC–IFN α 2 complex in a 1:1 molar ratio with respect to IFN α 2 and incubated for an additional 2 h. The binary and ternary complexes were then concentrated using Vivaspin concentrators (10 kDa molecular mass cutoff, GE Healthcare). The final concentration of the binary IFN α 2–IFNAR2-EC complex was 0.3 mM in 25 mM deuterated Tris in a 95% H_2O /5% D_2O solution (pH 8) containing 0.02% NaN_3 . The final concentration of the ternary complex was 0.2 mM in 25 mM deuterated Tris (pH 8) in a 95% H_2O /5% D_2O solution containing 0.02% NaN_3 and 150 mM NaCl. The binary and ternary complex solutions differed in the salt concentration since the binary complex was most stable without the addition of NaCl and the ternary complex containing IFNAR1-EC was most stable in the presence of 150 mM NaCl. Control HSQC measurements for evaluating the effect of NaCl on the chemical shifts of IFN α 2 were performed on samples containing 50 μM [^2H , ^{15}N]IFN α 2–U-IFNAR2-EC complex in 25 mM

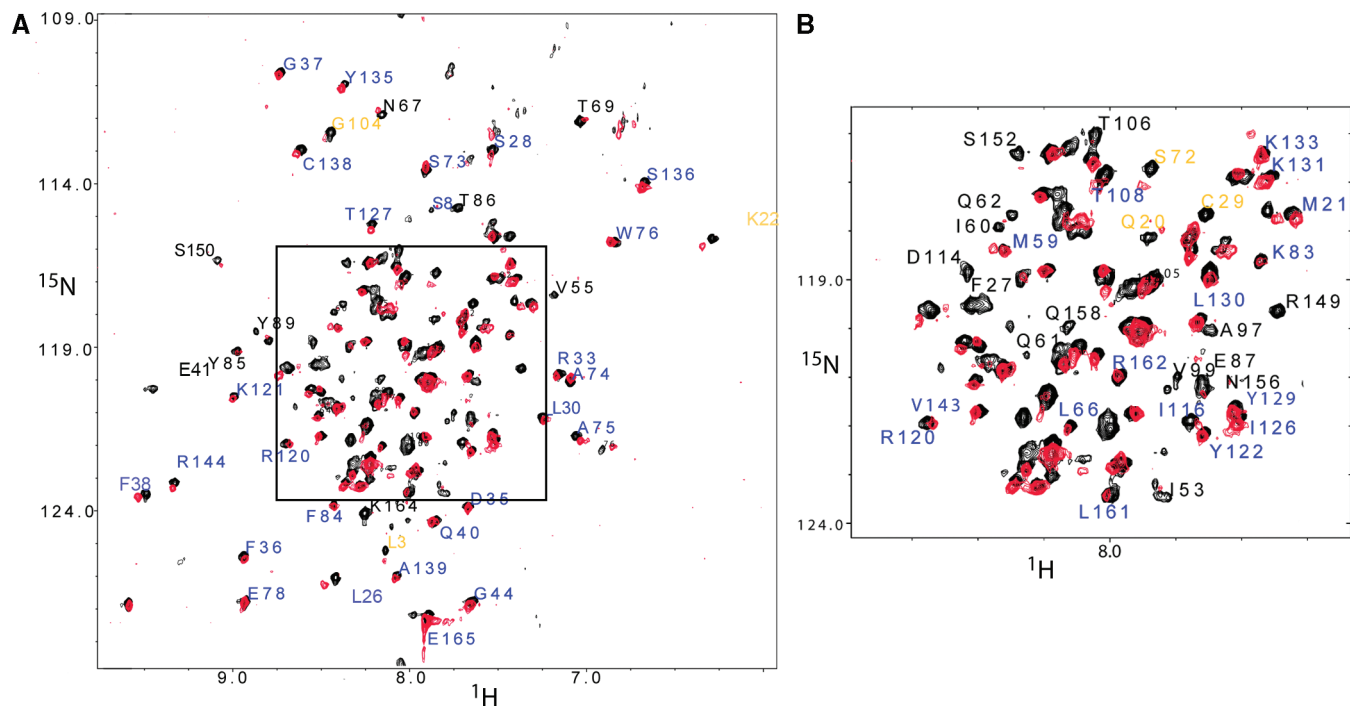


FIGURE 1: (A) Overlay of the ^{15}N – ^1H TROSY-HSQC spectra of the IFN α 2–IFNAR2-EC binary complex (black) and IFNAR1-EC–IFN α 2–IFNAR2-EC ternary complex (red) and (B) expansion of the central (boxed) region of this spectrum. Residues that did not change their chemical shift significantly upon IFNAR1-EC binding are labeled in blue, and residues that underwent significant changes in chemical shift upon IFNAR1-EC binding are labeled in yellow ($0.05 \text{ ppm} < \Delta\delta < 0.10 \text{ ppm}$); residues that could not be assigned due to large changes in chemical shift or disappearance upon IFNAR1-EC binding are labeled in black. Spectra were recorded at 308 K and pH 8.

deuterated Tris (pH 8) in a 95% H_2O /5% D_2O solution and 0.02% NaN_3 with or without 150 mM NaCl.

All NMR measurements were recorded at 308 K on a Bruker DRX 800 MHz spectrometer equipped with an x,y,z -gradient triple-resonance probe. Data were processed and analyzed using NMRPipe (36) and NMRView (37).

The two-dimensional (2D) ^1H – ^{15}N TROSY-HSQC spectra of the $[\text{}^2\text{H}, \text{}^{15}\text{N}]\text{IFN}\alpha 2$ –U-IFNAR2-EC and U-IFNAR1-EC– $[\text{}^2\text{H}, \text{}^{15}\text{N}]\text{IFN}\alpha 2$ –U-IFNAR2-EC complexes were acquired using 256 (160) t_1 increments with a sweep width of 1622 (1622) Hz and 1024 (1024) t_2 points with a sweep width of 10417 (10417) Hz. The number of scans in each experiment was 16 (16), and the relaxation delay was 1.4 s (2.0 s) (numbers in parentheses are those used for the ternary complex). Water flip-back and Watergate were used for water suppression. For the processing of the binary complex data, 256 t_1 increments (zero-filled to 512) and 700 t_2 points (zero-filled to 1400) were used. For the processing of the ternary complex data, 90 t_1 increments (zero-filled to 180) and 700 t_2 points (zero-filled to 1400) were used. In both spectra, a sine bell window function with a $\pi/2$ offset was used. The control 2D ^1H – ^{15}N TROSY-HSQC spectra of the $[\text{}^2\text{H}, \text{}^{15}\text{N}]\text{IFN}\alpha 2$ –U-IFNAR2-EC complex with and without NaCl were acquired using 96 scans. All other parameters were the same as described above. For the sake of simplicity, in what follows we will refer to ^1H – ^{15}N TROSY-HSQC as HSQC.

Sequence alignment was performed using ClustalW (38), and structure alignment of IFN α 2 and IFN β was performed using the Combinatorial Extension method (39) provided online at <http://cl.sdsc.edu/>. Molecular pictures were created using Pymol (40).

RESULTS

Changes in the TROSY-HSQC Spectrum of IFN α 2 in the IFN α 2–IFNAR2-EC Complex upon IFNAR1-EC

Binding. NMR is a very powerful technique for mapping the binding sites of proteins and assessing their conformational changes upon ligand binding. This can be achieved by measuring ^1H – ^{15}N HSQC spectra of the protein alone and in complex with its ligand, and subsequent analysis of the changes in chemical shifts as a result of ligand binding. Sequential assignment of the free protein is a prerequisite for this analysis in a residue specific manner. However, sequential assignment of the complex may not be necessary for determining the residues involved in ligand binding. This is especially advantageous when studying large ternary complexes such as the IFNAR1-EC–IFN α 2–IFNAR2-EC complex with a molecular mass of 102 kDa.

Deuteration of IFN α 2 considerably reduced the width of the IFN α 2 amide cross-peaks in the HSQC spectrum of the binary and ternary complexes. Nevertheless, we thought it would be beneficial to further reduce the line width of the resonances in the ternary complex. As it has been suggested that only the three N-terminal fibronectin domains of IFNAR1-EC (D1, D2, and D3) interact with IFN α 2 (5, 34) and since our labeling strategy in this study allowed observation of only changes in the cytokine, we used a construct of IFNAR1-EC missing the fourth domain (C domain), thus reducing the total size of the complex to 89 kDa and minimizing the change in the widths of the HSQC cross-peaks due to addition of the IFNAR1-EC protein.

Mapping of the binding site for IFNAR1-EC on free IFN α 2 was not possible since IFN α 2 aggregates under the conditions in which the binary IFNAR1-EC–IFN α 2 complex is stable (pH 7–8). In any case, the binding site for IFNAR1-EC on the binary IFNAR2-EC–IFN α 2 complex is more relevant since most probably IFN α 2 binds first to IFNAR2-EC and then recruits IFNAR1-EC to form the ternary complex (12, 13).

To map the binding site for IFNAR1-EC on the IFN α 2 molecule bound to IFNAR2-EC, we measured the HSQC spectra

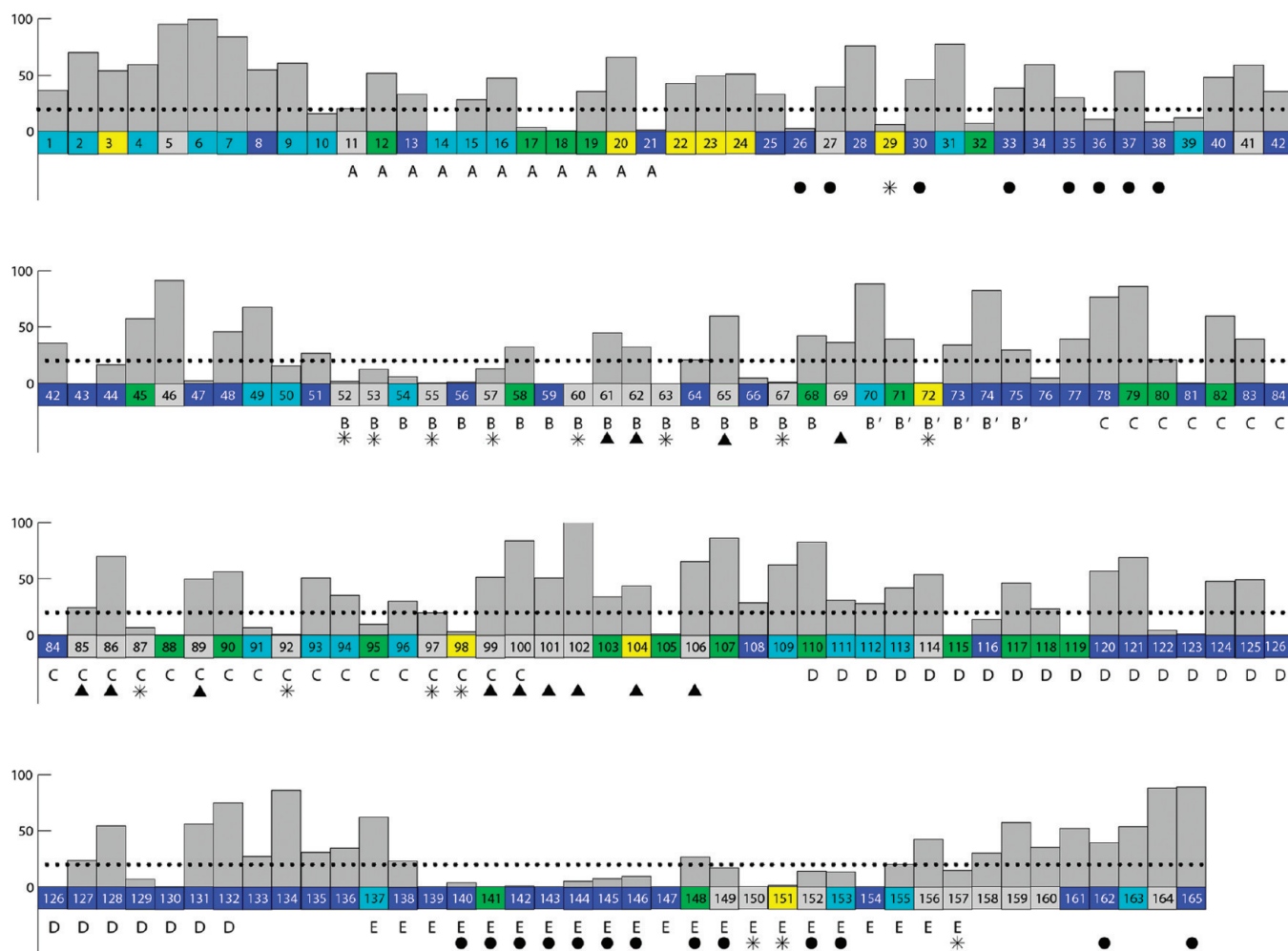


FIGURE 2: Summary of the changes in the IFN α 2 HSQC cross-peaks upon binding of IFNAR1-EC to the binary IFN α 2-IFNAR2-EC complex. Residues located in helices are marked with the corresponding helix label (A–E). Residues that did not change their chemical shift significantly upon IFNAR1-EC binding are colored deep blue, and residues that underwent significant chemical shift changes upon IFNAR1-EC binding are colored yellow (0.05 ppm < $\Delta\delta$ < 0.10 ppm). Residues that could not be assigned due to large chemical shift changes or disappearance upon IFNAR1-EC binding are colored gray, and overlapping cross-peaks that include one cross-peak that disappeared or underwent a large chemical shift change but could not be assigned due to overlap are colored green. Residues whose HSQC cross-peaks could not be assigned in the IFN α 2-IFNAR2-EC binary complex are colored cyan. The exposures of IFN α 2 residues (backbone and side chain included) in the binary complex are given by gray bars with a scale from 0 to 100%. A dotted line represents 20% exposure, and below this value of exposure, residues are defined as buried. Filled black triangles denote residues that are not buried and are implicated in IFNAR1-EC binding in this study. Buried residues that underwent significant changes in chemical shift or disappeared upon IFNAR1-EC binding and were not found to be involved in IFNAR2-EC binding are denoted with asterisks. Filled black circles denote residues found by NMR and site-directed mutagenesis to interact with IFNAR2-EC in the binary complex (4, 22, 24).

of uniformly ^2H - and ^{15}N -labeled IFN α 2 in complex with U-IFNAR2-EC before and after the addition of U-IFNAR1-EC under the same pH and temperature conditions. Measurements were taken in a 95% $\text{H}_2\text{O}/5\%$ D_2O solution to enable detection of the ^1H - ^{15}N amide cross-peaks in the HSQC spectra. It should be noted that sequential assignment for 85% of the amide ^1H and ^{15}N nuclei was previously obtained for IFN α 2 in complex with IFNAR2-EC at pH 8 and 308 K (24).

An overlay of HSQC spectra of the U-IFNAR1-EC-[^2H , ^{15}N]-IFN α 2-U-IFNAR2-EC ternary complex and the [^2H , ^{15}N]-IFN α 2-U-IFNAR2-EC binary complex is presented in Figure 1. The changes in chemical shift were calculated according to the formula $\Delta\delta = [(\Delta\text{N}/5)^2 + (\Delta\text{HN})^2]^{1/2}$. The majority of the unambiguously assigned amide HSQC cross-peaks of [^2H , ^{15}N]-IFN α 2 exhibited no changes or just small changes in chemical shift ($\Delta\delta < 0.05$ ppm) upon the formation of the ternary complex. This group contains 65 residues which are labeled and colored deep blue in Figures 1–3. A second group containing 10 residues

revealed significant changes in chemical shift (between 0.05 and 0.10 ppm, labeled and colored yellow in Figures 1–3). For a third group of residues, the HSQC cross-peaks either disappeared or could not be assigned in the ternary complex due to large differences in the chemical shifts of these IFN α 2 residues between the binary and ternary complexes. This group includes 37 residues which are labeled in black in Figure 1 and colored gray in Figures 2 and 3. For three of these 37 residues designated as “disappeared”, namely, N65, F67, and T69, the HSQC cross-peaks were weakened by 80, 72, and 87%, respectively, while the other 34 cross-peaks were not detected at all. In addition, there were two more groups of residues. The fourth group included IFN α 2 residues that could be assigned in the IFN α 2-IFNAR2-EC complex using three-dimensional (3D) NMR spectra; however, their HSQC cross-peaks showed overlap with cross-peaks of other residues. One of the overlapping cross-peaks either experienced a significant change in chemical shift or disappeared (these residues are colored green in Figures 2 and 3). The fifth group

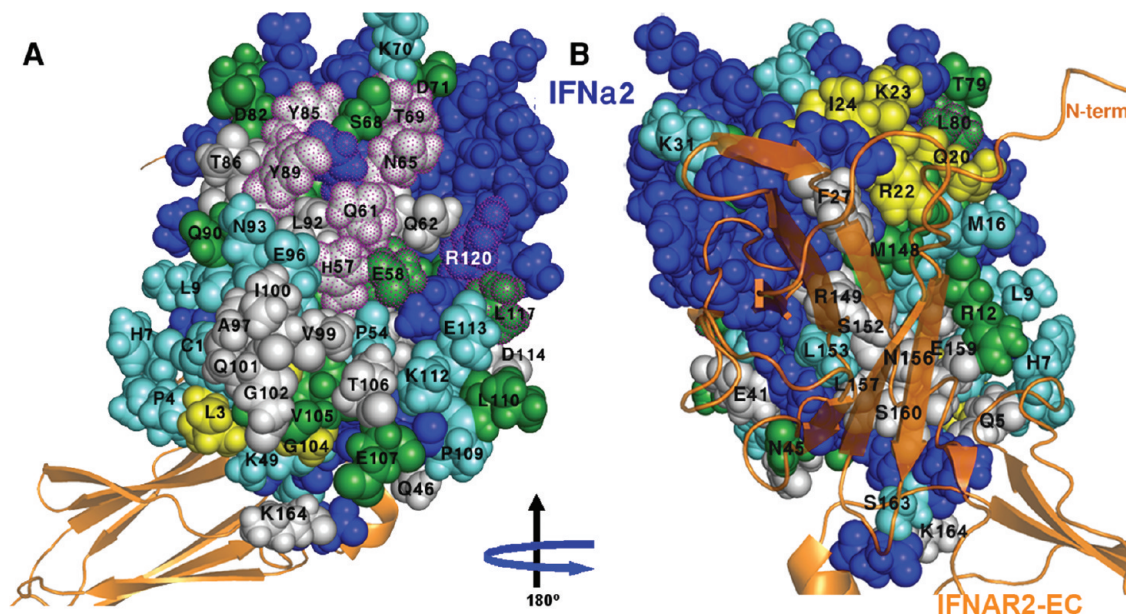


FIGURE 3: Mapping of the residues that exhibited significant chemical shift changes or disappeared upon binding of IFNAR1-EC on the surface of IFN α 2. (A) Face of IFN α 2 opposing the binding site for IFNAR2-EC that contains the two patches involved in IFNAR1-EC binding according to this study. (B) Face of IFN α 2 containing the surface previously found to be involved in IFNAR2-EC binding. IFNAR2-EC bound to IFN α 2 is presented by an orange ribbon diagram according to the previously calculated model of the binary complex (24). Residues previously identified by site-directed mutagenesis as being involved in IFNAR1-EC binding (25) are marked with dotted purple surfaces. Other color coding is the same as in Figure 2. All molecular pictures were created using Pymol (40).

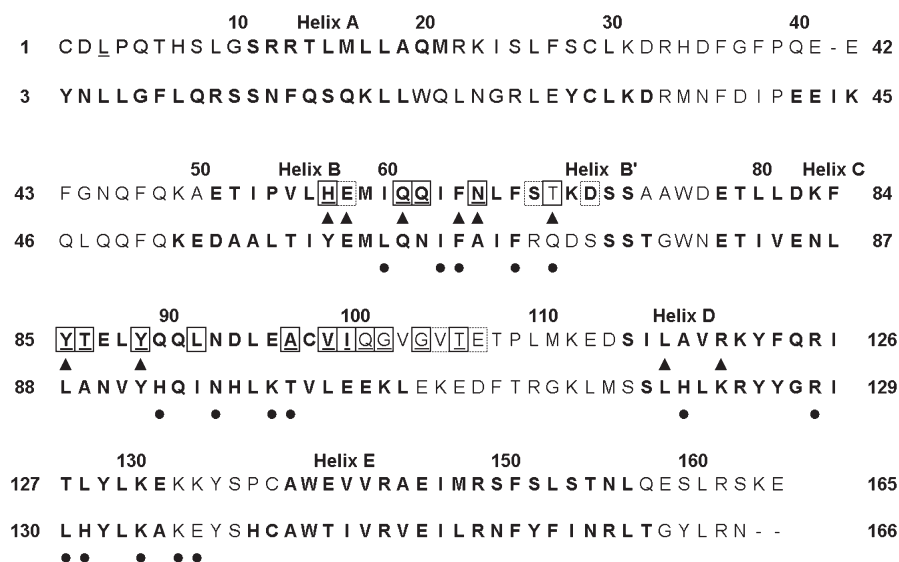


FIGURE 4: Comparison of IFN α 2 (top) and IFN β (bottom) residues implicated in IFNAR1-EC binding. Bold characters indicate IFN α 2 and IFN β residues found in the helices. Residues in boxes are IFN α 2 residues implicated in IFNAR1-EC binding in this study. Black triangles denote residues of IFN α 2 that were determined by mutagenesis to be in the binding site for IFNAR1-EC (25, 29). Filled black circles denote residues of IFN β that were determined by mutagenesis to be in the binding site of IFNAR1-EC (28).

included IFN α 2 residues whose HSQC cross-peaks could not be assigned in the IFN α 2–IFNAR2-EC binary complex (colored cyan in Figures 2 and 3). Residues from groups 1–5 were mapped on the structure of IFN α 2 (Figure 3). The sequence and secondary structure of IFN α 2 are presented in Figure 4.

The most significant change to the binary complex observed upon IFNAR1-EC binding is the disappearance of a large number of IFN α 2 cross-peaks in the HSQC spectrum of the complex. This change could be due to very large changes in chemical shift in IFN α 2 cross-peaks upon the formation of the ternary complex or broadening beyond detection of residues in the binding interface. In the HSQC spectrum of the binary complex, we counted

158 IFN α 2 cross-peaks, while in the ternary complex, 129 cross-peaks were counted, indicating that the vast majority of the 37 cross-peaks in group 3 (gray in Figures 2 and 3) actually vanished rather than changed their chemical shift upon IFNAR1-EC binding. The weak binding of IFNAR1-EC to the binary complex and its fast off rate (25) could contribute to the broadening of cross-peaks in the IFN α 2–IFNAR1-EC binding interface.

The binary and ternary complexes were measured using different NaCl concentrations (0 and 150 mM, respectively) due to sample stability issues. To determine whether the salt concentration had an effect on the chemical shifts of the binary IFN α 2–IFNAR2-EC complex, we measured HSQC spectra of

the [^2H , ^{15}N]IFN α 2–U-IFNAR2-EC complex with and without 150 mM NaCl at a low protein concentration (50 μM). Even at the low concentration that was used, we observed signal loss due to precipitation of the complex in the sample containing 150 mM NaCl. Nonetheless, we could clearly observe that the vast majority of cross-peaks was not affected by the addition of NaCl. Only two residues, L26 and F38, exhibited a minor change in chemical shift. This change in chemical shift due to the addition of salt was taken into account in our analysis of chemical shift changes between the binary and ternary complex.

Mapping the IFNAR1-EC Binding Site on IFN α 2. Earlier mutational studies identified the possible binding surface for IFNAR1-EC on the IFN face opposing the binding site for IFNAR2-EC (25, 29, 41). IFN α 2 residues that have the potential to interact with IFNAR1-EC must be exposed in the IFN α 2–IFNAR2-EC complex. The exposure of the IFN α 2 residues in the binary complex is shown in Figure 2 as gray bars. Figure 3 highlights residues whose chemical shifts were affected upon IFNAR1-EC binding. As shown in Figure 3A, the face of IFN α 2 opposing the binding site for IFNAR2-EC comprises a large exposed surface affected by IFNAR1-EC binding. This surface can be divided into two distinct areas. The upper surface contains residues Y85, T86, Y89, and L92 in the C helix, residues H57, Q61, Q62, and N65 in the B helix, and T69 which connects the B and B' helices. The lower adjacent surface contains residues A97, V99, and I100 in the C helix and Q101, G102, and T106 in the CD loop. Residues L3 and G104 which exhibit pronounced changes in chemical shift upon IFNAR1-EC binding (colored yellow in Figure 3) are adjacent to the second patch. On the basis of the changes in the HSQC spectrum, the exposure of many of the cytokine residues in these two surfaces, the involvement of the majority of the residues in the upper patch in IFNAR1 binding (25, 29, 41), and the proximity of the two surfaces, we suggest that both of these adjacent patches form the binding site for IFNAR1-EC.

Residues that are marked as “overlapping” are colored green in Figures 2 and 3. They are marked as such when one of two or three overlapping peaks exhibits a change in chemical shift upon IFNAR1-EC binding or when one of the peaks disappears, but due to cross-peak overlap, we could not conclude which of these was affected by IFNAR1-EC binding. Statistically, these residues have a 33–50% chance of being in the IFNAR1-binding interface. Not surprisingly, there are numerous such residues that are adjacent to the patches colored gray or yellow. One of these IFN α 2 residues, E58, has been implicated in IFNAR1 binding by site-directed mutagenesis studies (25). Other residues assigned as “overlapping” include S68, D71, D82, V105, and E107 that surround the surfaces identified in this study.

Changes in the HSQC Cross-Peaks of Residues in the Face of IFN α 2 Containing the Binding Site for IFNAR2-EC. The face of IFN α 2 on which the binding site for IFNAR2-EC is located contains eight residues that disappeared upon binding of IFNAR1-EC to the binary complex (colored gray in Figures 1–3) as well as four residues that significantly changed their chemical shift (colored yellow in Figures 1–3). These residues include Q20 at the end of the A helix, R22, K23, I24, and F27 in the AB loop, R149, S152, N156, and S157 in the E helix, E159 and S160 in the flexible C-terminal tail, and Q5 from the N-terminal tail. Of these residues, F27, R149, and S152 were previously identified by site-directed mutagenesis and by NMR as being in the IFN α 2-binding site for IFNAR2-EC (22–24). It

has been suggested that the flexible C-terminal tail is also involved in IFNAR2-EC binding in some IFNs (42).

Changes in the HSQC Cross-Peaks of Buried Residues. The HSQC spectrum of IFN α 2 in the binary complex contains many cross-peaks corresponding to buried residues (<20% exposure) that underwent significant changes upon binding of IFNAR1-EC (labeled with asterisks in Figure 2) and are not located in the binding sites for IFNAR1-EC and IFNAR2-EC. These residues include C29 in the AB loop, T52, I53, V55, I60, Q63, and F67 in the B helix, S72 in the B' helix, E87, L92, A97 (19.7% exposure), and C98 in the C helix, and S150, F151, and L157 in the E helix. The changes in the HSQC cross-peaks of these residues indicate that they are located in internal regions of the protein that underwent some changes in their environment or conformation upon IFNAR1-EC binding. Changes in local structure, which result in changes in chemical shifts, are necessary to facilitate the proposed allosteric interaction between the IFNAR1-EC and IFNAR2-EC binding interfaces.

DISCUSSION

Mapping the Binding Site for IFNAR1-EC. The mapping of the binding site for IFNAR1-EC on IFN α 2 bound to IFNAR2-EC presents a major challenge for NMR investigations because of the high molecular mass of the ternary complex (89 and 102 kDa for the complex with three and four IFNAR1-EC domains, respectively), the low concentration of the binary and ternary complexes that are soluble in aqueous solution (0.2 mM), the helical structure of IFN α 2 that results in considerable overlap in the HSQC spectrum, and the high pH at which the binary and the ternary complexes are stable (pH 8), resulting in fast exchange of exposed amide protons.

To map the binding site for IFNAR1-EC on IFN α 2, we analyzed the perturbation in the ^1H and ^{15}N chemical shifts of IFN α 2 bound to IFNAR2-EC upon the formation of the IFNAR1-EC–IFN α 2–IFNAR2-EC ternary complex. The HSQC spectrum of the ternary complex revealed that the cross-peaks of 34 residues vanished and three others experienced a considerable reduction in intensity. Only a small number of residues (10 residues) exhibited changes in chemical shifts upon IFNAR1-EC binding, and these changes were rather small (<0.1 ppm), indicating that they correspond to residues in the periphery of the regions affected by IFNAR1-EC binding.

Chemical shift perturbation is an indirect method for the identification of residues involved in the binding interface. Changes in chemical shift can be the result of direct binding or of other effects, such as allosteric changes, conformational changes upon binding, etc. Other NMR methods like cross saturation transfer or deuterium exchange would allow the identification of residues directly involved in binding. However, these methods were not suitable for the IFNAR1-EC–IFN α 2–IFNAR2-EC system, since most of the cross-peaks that were affected by IFNAR1-EC binding disappeared beyond detection in the ternary complex (37 residues).

By comparing the HSQC spectra of the binary and ternary complexes of IFN α 2, we were able to map two main surfaces of IFN α 2 that were affected upon the binding of IFNAR1-EC to the binary IFN α 2–IFNAR2-EC complex. One surface that consists of two adjacent large patches is implicated in IFNAR1-EC binding, and the other is located on the face of IFN α 2 containing the binding site for IFNAR2-EC.

The upper section of the surface involved in IFNAR1-EC binding (Figure 3) consists of exposed residues at the center and

C-terminal end of the B helix as well as residues at the center of the C helix (Figure 2). This patch overlaps very well with the IFNAR1-EC binding surface previously identified by site-directed mutagenesis which suggested that residues H57, E58, Q61, F64, N65, and T69 in the B helix and L80, Y85, and Y89 located in the C helix are involved in the binding of IFNAR1-EC to IFN α 2 (25). This study adds residues Q62, T86, and L92 to this site, resulting in a significant increase in the size of the protein–protein interface.

The NMR analysis could not confirm the involvement of L117 and R120 in IFNAR1-EC binding. These two residues were found to be involved in IFNAR1-EC binding by site-directed mutagenesis experiments. Mutation of residue L117, located in the D helix, resulted in a decrease in antiviral and antiproliferative activities (29). Unfortunately, the cross-peak for L117 overlaps with that of L88, and the cross-peak of one of these residues (it is not known which of them) exhibits changes in chemical shift upon IFNAR1-EC binding. Residue R120, located adjacent to residues E58, Q62, E113, and L117, was previously implicated in IFNAR1-EC binding (29). The R120A mutation and the R120E charge-reversal mutation significantly decreased the antiviral and antiproliferative activity of IFN α 2. However, no significant change in chemical shift upon IFNAR1-EC binding was observed for R120. Thus, R120 may play a structurally significant role rather than being involved in binding IFNAR1-EC directly.

The lower part of the IFN α 2 binding site for IFNAR1-EC includes L3 in the N-terminal segment, A97, V99, and L100 in the C-terminal end of the C helix, and Q101, G102, G104, and T106 in the CD loop. This patch has not been implicated in IFNAR1-EC binding previously. We suggest that this large surface containing six residues that disappeared upon IFNAR1-EC binding and two residues that significantly changed their chemical shift is involved in IFNAR1-EC binding in addition to the upper patch. Support for the existence of two IFN α 2 patches involved in IFNAR1-EC binding comes from the observation that two of the four fibronectin domains of IFNAR1-EC are major contributors to IFN binding (43). This was later demonstrated also by the EM-derived model for the ternary complex (34). It could be that one of the two patches identified in this study interacts with one of IFNAR1-EC fibronectin domains while the other cytokine patch interacts with a second IFNAR1-EC fibronectin domain similar to what has been suggested by the model for the ternary complex that was based on cryo-EM (see below and ref 34).

We also obtained evidence that binding of IFNs to IFNAR1-EC involves more than a single localized region of the cytokine by studying binding of IFNAR1-EC to IFN β . A systematic mutational analysis of human IFN β suggests the involvement of residues in the B helix (L63, I66, F67, and F70), the B' helix (Q72), the C helix (H93, N96, K99, and T100), and the D helix (H121, R128, L130, H131, and K134) as well as in the DE loops (K136 and E137) in the binding to IFNAR1-EC (28) (see Figure 4).

Sequence alignment (Figure 4) of IFN α 2 and IFN β (Figure 4) shows that the binding site for IFNAR1-EC on IFN α 2 identified by NMR partially overlaps with the binding site of IFNAR1-EC on IFN β determined by site-directed mutagenesis (28). The involvement of the B and C helices of IFN β in IFNAR1-EC binding agrees with our NMR study. However, the binding site on IFN β involves also residues in the D helix and the DE loop which showed no changes in the HSQC spectrum of IFN α 2 upon IFNAR1-EC binding.

Comparison with the EM Structure of IFNAR2-EC–IFN α 2–IFNAR1-EC Ternary Complex. A model for the three-dimensional structure of the IFNAR2-EC–IFN α 2–IFNAR1-EC ternary complex was previously obtained (34) using the NMR-derived model for the IFNAR2-EC–IFN α 2 binary complex (24), and a homology model for IFNAR1-EC fitted into the low-resolution electron density map of the ternary complex (34). Although the model of the ternary complex was not obtained on the basis of specific interactions between IFNAR1-EC and IFN α 2, the fitting of the homology model of IFNAR1-EC into the EM structure is revealing in terms of identifying regions that could potentially participate in IFNAR1-EC binding. Overall, the model suggests that three regions of IFN α 2 are involved in IFNAR1-EC binding, and these are (a) the N-terminal flexible tail of IFN α 2, (b) the B helix, and (c) the C helix (mainly residues 92–100) and the CD loop (34). Indeed, L3 and Q5 underwent changes in the HSQC spectrum upon binding of IFNAR1-EC to the binary complex. However, most of the N-terminal tail residues could not be assigned. Therefore, there is no firm conclusion in this study regarding the involvement of the N-terminus of the cytokine in the interaction with IFNAR1. Region b overlaps the B helix surface implicated in IFNAR1-EC binding in this study. Region C coincides with the large patch containing V99, I100, Q101, G102, and T106 found to be involved in IFNAR1-EC binding in this study, thus providing further support that this patch is involved in IFN α 2 binding rather than disappearing because of conformational changes.

Allostery in the Binding of IFNAR1 to the IFN α 2–IFNAR2-EC Complex. Binding of IFNAR1-EC to the IFN α 2–IFNAR2-EC binary complex caused significant changes in the cross-peaks of IFN α 2 residues in the face of the molecule that contains the binding site for IFNAR2-EC. This patch includes three IFN α 2 residues that were previously implicated in IFNAR2-EC binding by saturation-transfer experiment (F27, R149, and S152) (see Figure 2 and ref 24). IFN α 2 residues N156, L157, Q158, E159, and S160 form a patch of five residues whose cross-peaks disappeared upon binding of IFNAR1-EC to the IFN α 2–IFNAR2-EC binary complex. This patch is flanked on one side by R149 and S152 and on the other side by R162 and E165 that were previously found to be involved in IFNAR2-EC binding in the NMR-derived model for the binary complex (24).

Figure 5 shows the proximity between the IFN α 2 C-terminal tail and IFNAR2-EC. The shortest distances between N156, E159, and S160 and IFNAR2-EC atoms are 3.0, 8.0, and 6.0 Å, respectively. It has been reported that mutations in the C-terminal tail caused an up to 20-fold difference in the binding affinity of IFNs for IFNAR2-EC (41). Although this tail does not contribute significantly to IFN α 2 binding to IFNAR2-EC, it does contribute to IFN α 8 binding to IFNAR2-EC (42). It has been suggested that the flexible C-terminal tail becomes structured upon IFNAR2-EC binding (42). As shown in Figure 5, IFN α 2 residues N156, E159, and S160 could potentially interact with the β 9– β 10 and/or β 13– β 14 loops of IFNAR2-EC if IFN α 2 was tilted slightly toward the C fibronectin domain of IFNAR2-EC or if the flexible IFN α 2 C-terminal tail adopted a structure that brought it closer to IFNAR2-EC. Therefore, we propose that the IFN α 2 binding site for IFNAR2-EC undergoes allosteric conformational changes when IFNAR1-EC binds to the IFN α 2–IFNAR2-EC binary complex.

Ten residues of 17 in the IFN α 2 B helix disappeared when IFNAR1-EC bound to the binary complex. Of these 10 residues, only three, namely, Q61, Q62, and N65, are exposed, and H57 is

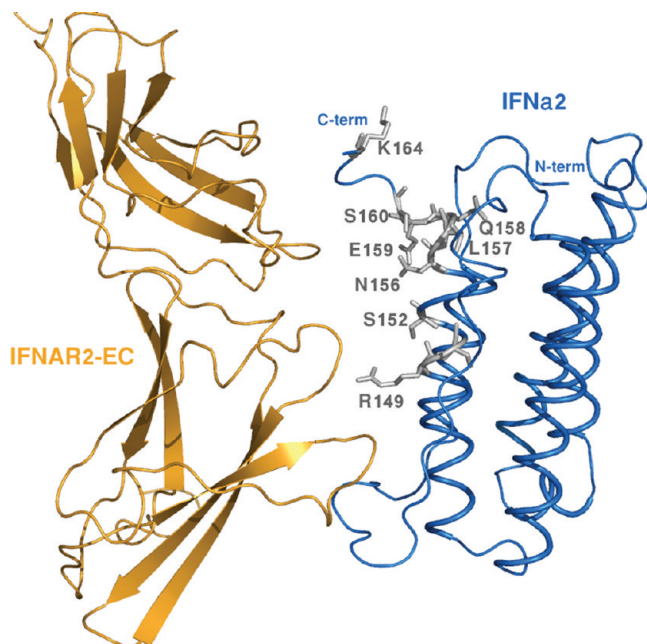


FIGURE 5: Side view of the IFN α 2–IFNAR2-EC binding interface. IFN α 2 and IFNAR2-EC are colored blue and orange, respectively. The E helix and the C-terminal tail residues that disappeared when IFNAR1-EC bound to the binary complex are shown in stick representation and colored gray.

marginally exposed (17%). The other six residues within the B helix that disappeared upon IFNAR1-EC binding are buried. The disappearance of such a large number of buried residues indicates that the B helix, which forms together with the E helix the center of the five-helix bundle, undergoes significant movement upon binding of IFNAR1-EC to the binary complex. Interestingly also, six residues of the nine-residue C-terminal segment of the E helix undergo considerable changes in chemical shift or disappear upon IFNAR1-EC binding. Of these six residues, four are buried and do not interact with IFNAR2-EC. It is plausible that these changes in the central helices B and E reflect their involvement in modulating the allosteric changes in IFN α 2 that are transmitted to the IFNAR2-EC binding site. This movement could involve also the C helix.

The allosteric changes in the IFNAR2-EC binding site caused by IFNAR1-EC binding might affect the orientation of IFNAR2 with respect to IFNAR1 and thereby influence the cross phosphorylation of the IFNAR1-associated Tyk2 protein and the IFNAR2-associated Jak1. These phosphorylations initiate the intracellular signal transduction cascade leading to the antiviral and antiproliferative response to interferon.

In a previous study, we reported that H57 and adjacent residues (V55, M59, V60, Y89, and E96) undergo chemical shift changes upon binding of IFNAR2-EC to IFN α 2 (24). These residues are located on the face of IFN α 2 opposing the binding site for IFNAR2-EC. Of these residues, H57, V60, and Y89 were mapped in this study as being in the binding site for IFNAR1-EC. However, in the earlier investigation, we could not draw any firm conclusion regarding allostery since the free IFN α 2 spectrum was recorded at pH 3.5 and that of the IFN α 2–IFNAR2-EC binary complex was recorded at pH 8.0. A change in the protonation state of H57 could well have been the reason for the observed changes in its chemical shift between IFN α 2 and the IFN α 2–IFNAR2-EC complex. This study provides unequivocal evidence of the existence of an allosteric interaction between

IFNAR1-EC and IFNAR2-EC binding sites mediated by the IFN α 2 cytokine since all HSQC spectra were recorded under the same conditions.

Conclusions. This study together with previous site-directed mutagenesis and EM studies suggests that the binding site for IFNAR1-EC on IFN α 2 consists of two large patches located on the IFN α 2 face opposing the binding site for IFNAR2-EC. Most importantly, the NMR study presented here provides an unequivocal indication of the communication between the IFN α 2 binding sites for IFNAR1-EC and IFNAR2-EC resulting in some change in conformation in the binding site for IFNAR2-EC caused by IFNAR1-EC binding. These conformational changes caused by allosteric effects, which might be translated to the cytoplasmic part of the receptor, likely play an important role in the initiation of the intracellular signal transduction cascade.

ACKNOWLEDGMENT

We are most grateful to Ms. Rina Levy for the preparation of IFNAR2-EC and labeled IFN α 2 and to Dr. Fred Naider for extensive discussions and comments on the manuscript.

REFERENCES

1. Pestka, S., Krause, C. D., and Walter, M. R. (2004) Interferons, interferon-like cytokines, and their receptors. *Immunol. Rev.* 202, 8–32.
2. Novick, D., Cohen, B., and Rubinstein, M. (1994) The human interferon α/β receptor: Characterization and molecular cloning. *Cell* 77, 391–400.
3. Uze, G., Lutfalla, G., and Mogensen, K. E. (1995) α and β interferons and their receptor and their friends and relations. *J. Interferon Cytokine Res.* 15, 3–26.
4. Piehler, J., and Schreiber, G. (1999) Mutational and structural analysis of the binding interface between type I interferons and their receptor Ifnar2. *J. Mol. Biol.* 294, 223–237.
5. Lamken, P., Gavutis, M., Peters, I., Van der Heyden, J., Uze, G., and Piehler, J. (2005) Functional cartography of the ectodomain of the type I interferon receptor subunit ifnar1. *J. Mol. Biol.* 350, 476–488.
6. Ozbek, S., Grotzinger, J., Krebs, B., Fischer, M., Wollmer, A., Jostock, T., Mullberg, J., and Rose-John, S. (1998) The membrane proximal cytokine receptor domain of the human interleukin-6 receptor is sufficient for ligand binding but not for gp130 association. *J. Biol. Chem.* 273, 21374–21379.
7. Cunningham, B. C., Ultsch, M., De Vos, A. M., Mulkerrin, M. G., Clauser, K. R., and Wells, J. A. (1991) Dimerization of the extracellular domain of the human growth hormone receptor by a single hormone molecule. *Science* 254, 821–825.
8. Gent, J., Van Kerkhof, P., and Strous, G. J. (2003) Dimerization and signal transduction of the growth hormone receptor. *Mol. Endocrinol.* 17, 967–975.
9. Krause, C. D., and Pestka, S. (2005) Evolution of the Class 2 cytokines and receptors, and discovery of new friends and relatives. *Pharmacol. Ther.* 106, 299–346.
10. Bernat, B., Pal, G., Sun, M., and Kossiakoff, A. A. (2003) Determination of the energetics governing the regulatory step in growth hormone-induced receptor homodimerization. *Proc. Natl. Acad. Sci. U.S.A.* 100, 952–957.
11. Remy, I., Wilson, I. A., and Michnick, S. W. (1999) Erythropoietin receptor activation by a ligand-induced conformation change. *Science* 283, 990–993.
12. Gavutis, M., Lata, S., Lamken, P., Muller, P., and Piehler, J. (2005) Lateral ligand-receptor interactions on membranes probed by simultaneous fluorescence-interference detection. *Biophys. J.* 88, 4289–4302.
13. Gavutis, M., Jaks, E., Lamken, P., and Piehler, J. (2006) Determination of the two-dimensional interaction rate constants of a cytokine receptor complex. *Biophys. J.* 90, 3345–3355.
14. Karpusas, M., Nolte, M., Benton, C. B., Meier, W., Lipscomb, W. N., and Goetz, S. (1997) The crystal structure of human interferon β at 2.2-Å resolution. *Proc. Natl. Acad. Sci. U.S.A.* 94, 11813–11818.
15. Senda, T., Shimazu, T., Matsuda, S., Kawano, G., Shimizu, H., Nakamura, K. T., and Mitsui, Y. (1992) Three-dimensional crystal

- structure of recombinant murine interferon- β . *EMBO J.* 11, 3193–3201.
16. Klaus, W., Gsell, B., Labhardt, A. M., Wipf, B., and Senn, H. (1997) The three-dimensional high resolution structure of human interferon α -2a determined by heteronuclear NMR spectroscopy in solution. *J. Mol. Biol.* 274, 661–675.
17. Radhakrishnan, R., Walter, L. J., Hruza, A., Reichert, P., Trotta, P. P., Nagabhushan, T. L., and Walter, M. R. (1996) Zinc mediated dimer of human interferon- α 2b revealed by X-ray crystallography. *Structure* 4, 1453–1463.
18. Radhakrishnan, R., Walter, L. J., Subramaniam, P. S., Johnson, H. M., and Walter, M. R. (1999) Crystal structure of ovine interferon- τ at 2.1 Å resolution. *J. Mol. Biol.* 286, 151–162.
19. Chill, J. H., Quadt, S. R., Levy, R., Schreiber, G. E., and Anglister, J. (2003) NMR structure of the human type I interferon receptor reveals the molecular basis for ligand binding. *Structure* 11, 791–802.
20. Chill, J. H., Quadt, S. R., and Anglister, J. (2004) NMR backbone dynamics of the human type I interferon binding subunit, a representative cytokine receptor. *Biochemistry* 43, 10127–10137.
21. Chuntharapai, A., Gibbs, V., Lu, J., Ow, A., Marsters, S., Ashkenazi, A., De Vos, A., and Jin Kim, K. (1999) Determination of residues involved in ligand binding and signal transmission in the human IFN- α receptor 2. *J. Immunol.* 163, 766–773.
22. Roisman, L. C., Piehler, J., Trosset, J.-Y., Scheraga, H. A., and Schreiber, G. E. (2001) Structure of the interferon-receptor complex determined by distance constraints from double mutant cycles and flexible docking. *Proc. Natl. Acad. Sci. U.S.A.* 98, 13231–13236.
23. Piehler, J., Roisman, L. C., and Schreiber, G. (2000) New structural and functional aspects of the IFN-receptor interaction revealed by comprehensive mutational analysis of the binding interface. *J. Biol. Chem.* 275, 40425–40433.
24. Quadt-Akabayov, S. R., Chill, J. H., Levy, R., Kessler, N., and Anglister, J. (2006) Determination of the human type I interferon receptor binding site on human interferon- α 2 by cross saturation and an NMR-based model of the complex. *Protein Sci.* 15, 2656–2668.
25. Roisman, L. C., Jaitin, D. A., Baker, D. P., and Schreiber, G. (2005) Mutational analysis of the IFNAR1 binding site on IFN α 2 reveals the architecture of a weak ligand-receptor binding-site. *J. Mol. Biol.* 353, 271–281.
26. Stroud, R. M., and Wells, J. A. (2004) Mechanistic diversity of cytokine receptor signaling across cell membranes. *Sci. STKE* 2004, re7.
27. Hu, R., Bekisz, J., Schmeisser, H., McPhie, P., and Zoon, K. (2001) Human IFN- α protein engineering: The amino acid residues at positions 86 and 90 are important for antiproliferative activity. *J. Immunol.* 167, 1482–1489.
28. Runkel, L., deDios, C., Karpusas, M., Betzenhauser, M., Muldowney, C., Zafari, M., Benjamin, C. D., Miller, S., Hochman, P. S., and Whitty, A. (2000) Systematic mutational mapping of sites on human interferon- β -1a that are important for receptor binding and functional activity. *Biochemistry* 39, 2538–2551.
29. Pan, M., Kalie, E., Scaglione, B. J., Raveche, E. S., Schreiber, G., and Langer, J. A. (2008) Mutation of the IFNAR-1 receptor binding site of human IFN- α 2 generates type I IFN competitive antagonists. *Biochemistry* 47, 12018–12027.
30. Jaitin, D. A., Roisman, L. C., Jaks, E., Gavutis, M., Piehler, J., Van der Heyden, J., Uze, G., and Schreiber, G. (2006) Inquiring into the differential action of interferons (IFNs): An IFN- α 2 mutant with enhanced affinity to IFNAR1 is functionally similar to IFN- β . *Mol. Cell. Biol.* 26, 1888–1897.
31. Kalie, E., Jaitin, D. A., Abramovich, R., and Schreiber, G. (2007) An interferon α 2 mutant optimized by phage display for IFNAR1 binding confers specifically enhanced antitumor activities. *J. Biol. Chem.* 282, 11602–11611.
32. Cutrone, E. C., and Langer, J. A. (2001) Identification of critical residues in bovine IFNAR-1 responsible for interferon binding. *J. Biol. Chem.* 276, 17140–17148.
33. Cajean-Feroldi, C., Nosal, F., Nardeux, P. C., Gallet, X., Guymarho, J., Baychelier, F., Sempe, P., Tovey, M. G., Escary, J. L., and Eid, P. (2004) Identification of residues of the IFNAR1 chain of the type I human interferon receptor critical for ligand binding and biological activity. *Biochemistry* 43, 12498–12512.
34. Li, Z., Strunk, J. J., Lamken, P., Piehler, J., and Walz, T. (2008) The EM structure of a type I interferon-receptor complex reveals a novel mechanism for cytokine signaling. *J. Mol. Biol.* 377, 715–724.
35. Chill, J. H., Nivasch, R., Levy, R., Albeck, S., Schreiber, G. E., and Anglister, J. (2002) The human interferon receptor: NMR-based modeling of the IFN- α 2 binding site, and observed ligand-induced tightening. *Biochemistry* 41, 3575–3585.
36. Delaglio, F., Grzesiek, S., Vuister, G. W., Zhu, G., Pfeifer, J., and Bax, A. (1995) Nmrpipe: A Multidimensional Spectral Processing System Based On Unix Pipes. *J. Biomol. NMR* 6, 277–293.
37. Johnson, B. A., and Blevins, R. A. (1994) NMRView: A computer program for the visualization and analysis of NMR data. *J. Biomol. NMR* 4, 603–614.
38. Larkin, M. A., Blackshields, G., Brown, N. P., Chenna, R., McGettigan, P. A., McWilliam, H., Valentin, F., Wallace, I. M., Wilm, A., Lopez, R., Thompson, J. D., Gibson, T. J., and Higgins, D. G. (2007) Clustal W and Clustal X version 2.0. *Bioinformatics* 23, 2947–2948.
39. Shindyalov, I. N., and Bourne, P. E. (1998) Protein structure alignment by incremental combinatorial extension (CE) of the optimal path. *Protein Eng.* 11, 739–747.
40. DeLano, W. L. (2002) The PyMOL Molecular Graphics System, DeLano Scientific, Palo Alto, CA.
41. Uze, G., Schreiber, G., Piehler, J., and Pellegrini, S. (2007) The receptor of the type I interferon family. *Curr. Top. Microbiol. Immunol.* 316, 71–95.
42. Slutzki, M., Jaitin, D. A., Yehezkel, T. B., and Schreiber, G. (2006) Variations in the unstructured C-terminal tail of interferons contribute to differential receptor binding and biological activity. *J. Mol. Biol.* 360, 1019–1030.
43. Goldman, L. A., Cutrone, E. C., Dang, A., Hao, X., Lim, J. K., and Langer, J. A. (1998) Mapping human interferon- α (IFN- α 2) binding determinants of the type I interferon receptor subunit IFNAR-1 with human/bovine IFNAR-1 chimeras. *Biochemistry* 37, 13003–13010.